[1]Vidya Patil

[2]Anuradha Phadke

[3]Subrata Kumar Das

Hue Channel Mesoscale Convective System Identification Techniques using Kalpana Geostationary Satellite Observations

Journal of Electrical Systems

Abstract: - Climate change is leading to sudden extreme weather events like floods and heavy rain to occur. One of the most significant rain-bearing systems, Mesoscale Convective Systems (MCSs), is in charge of catastrophic rainfall and flood events that may cause loss of life and property. MCSs are one of the vital components of the climate system on Earth. Many studies contributed to two significant steps, MCS identification and tracking. There are a variety of algorithms focused on tracking whereas for MCS identification only limited methods are present. They contribute to global as well as regional climate patterns by transporting heat and moisture. It is necessary to identify MCS properly to track MCS occurrences over time and comprehend their typical lifecycle to get early warnings of their existence. Three MCS identification techniques based on the Hue channel of the Hue Saturation Value (HSV) color model are implemented in this research, and their effectiveness is assessed. These techniques execute segmentation based on Hue channel Thresholding (HT), K means clustering combined with Hue channel Thresholding (KMCHT) and the modified Source Apportionment Technique combined with Hue channel Thresholding (SATHT). Image pixel values are used to depict infrared brightness temperature data obtained from the Indian geostationary satellite Kalpana-1. The generated ground truth images and performance measurements are used to assess the effectiveness of the methods. The proposed SATHT method for multiple cloud segmentation results in superior performance metrics than the HT and KMCHT approaches.

Keywords: Identification, Mesoscale Convective Systems, Segmentation, Thresholding

I. INTRODUCTION

Mesoscale Convective Systems (MCSs) represent cloud clusters holding a group of thunderstorms, within it causing contiguous precipitation over an area covering approximately 100 km along the horizontal scale in one direction [1]. Prolific rainmakers, MCSs possess the capacity to generate large amounts of precipitation within a short duration leading to floods, which may cause property damage and loss of life [1] [3]. Sometimes MCS existence can be the reason for occurrences of tornadoes and hail [3]. In most parts of the tropical belt, such as the Bay of Bengal, Indo-Pacific warm pool, tropical Eastern Pacific, and tropical Eastern Atlantic, MCS precipitation contributions exceed 50% of yearly total precipitation [2]. Over the Indian subcontinent, the MCS rainfall portion ranges from 40%-60%. Therefore, it is important to understand and study the MCSs characteristics considering their hazardous existence. In order to improve weather forecasting models and enhance the understanding of atmospheric processes, MCSs are the focus of significant research [1]. Forecasts of rainfall, severe weather, and other meteorological phenomena is made easier by studying MCSs. Major research has been conducted on MCS identification, characterization, and tracking using advanced remote sensing technology. Geostationary meteorological satellite infrared imagery data has been globally used to study the MCS due to its wide space and time coverage [3], [4]. Maddox [5] initiated the MCS studies in the United States and identified Mesoscale Convective Complexes (MCCs). Using satellite images, the MCS climatology was documented over the Indian monsoon and globally [6]. MCS characteristics were further examined in other regions, including South America, Africa, South Asia, and the Maritime continent [2] [3] [4] [6] [7]. Most of the MCS characteristics and organization investigation is carried out with brightness temperature (BT) based thermal infrared (IR) images as pixel intensities in an image are directly proportional to the cloud temperature.

Though MCS cloud identification is a significant step for MCS area coverage calculation, the existing literature

[1]Dr. Vishwanath Karad MIT World Peace University, Department of Electrical and Electronics Engineering Pune, India

vidya.patil@mitwpu.edu.in

[2]Dr. Vishwanath Karad MIT World Peace University, Department of Electrical and Electronics Engineering Pune, India

anuradha.phadke@mitwpu.edu.in

[3]Ministry of Earth Sciences, Indian Institute of Tropical Meteorology Pune, India

subrata@tropmet.res.in

lacks analysis and comparison of the methods used for it. In this research work, MCS are identified from RGB color maps generated using IR BT data taken from the Indian geostationary satellite, Kalpana-1. The objective of the paper is to focus on detecting or identifying MCS based on IR BT observations using three techniques, Hue channel Thresholding (HT), *K* means clustering combined with Hue channel Thresholding (KMCHT), and the modified Source Apportionment Technique combined with Hue channel Thresholding (SATHT) and comparison of their results due to its importance in understanding the MCS occurrence patterns. This study contributed a combination of the Source Apportionment Technique (SAT) and the Thresholding technique to identify multiple cloud clusters in an image. Results are compared using performance metrics such as Mean Intersection of Union (IoU), Mean Pixel Accuracy, Mean Precision, Mean Recall, and Mean F1 score along with execution time. These results will be compared with the results of Deep Learning (DL) based algorithms to assess and confirm the worthiness of DL techniques used for cloud segmentation as it involves a substantial amount of cost, time as well as effort for the creation of labelled data.

The paper is organised as, the literature review in section 2, Data set and methods in section 3, Results and discussions are given in section 4, and section 5 concludes the work.

II. LITERATURE REVIEW

Many studies contributed to two significant steps, MCS identification and their tracking using IR BT data from geostationary satellites [3] [4] [5] [7] [8] [9] [10] [11] [12]. There are a variety of algorithms focused on tracking whereas for MCS identification only limited methods are present. IR BT threshold and the minimum size requirements were used for MCS identification. The temperature and size criteria were chosen arbitrarily, and they vary according to the specific MCS type and study location [10] [11] [12]. A detailed review of different methods and studies for MCS identification, also known as detection and tracking is available in [13]. These studies highlighted the significance of MCS identification. Various temperature thresholds ranging from 190–258K have been used to detect MCSs [10]. Some studies used a single temperature threshold, while others given in employed several temperature thresholds (190-235K) to identify MCS [8] [14]. Most studies used a BT threshold within the range of 228-263K and around 220K or less, where deep convection is considered as a single threshold value or combination of multiple thresholds [2] [4] [10] [11] [12] [15] [16] [17]. Thresholding-based segmentation depending on IR BT is an inherent part of the MCS identification step. The above points highlight that MCS identification is often made using cloud segmentation based on the Thresholding technique.

Although the Thresholding method is often used for MCS identification, there are other additional approaches also found in the literature. Reference [7] identified MCSs using the Source Apportionment Technique (SAT). It works only with one global minimum BT within the domain of interest for single MCS extraction, but several local minima might exist within an image. Reference [18] used a fuzzy min-max neural network to identify the cold clouds representing MCS. The Thresholding approach is used in conjunction with other techniques in [19] and [20]. References [8] and [21] employed three-dimensional (3D) segmentation with varied BT threshold values to obtain 3D cloud clusters of varying temperatures separately as part of the Tracking of Organized Convection Algorithm through a 3-D segmentatioN algorithm (TOOCAN). The *K* means clustering (KMC) algorithm is also used to identify the convective clouds in [22] [23] [24]. Reference [25] identified MCS as a Gaussian mixture represented by a 2D spheroid. As mentioned earlier, MCS identification in all techniques starts with the Thresholding technique, either directly or indirectly. Hence, it underlines the importance of the Thresholding technique for accurate MCS detection. Therefore, the Thresholding technique for cloud identification can be considered a State-of-the-art (SOTA) or base method for MCS identification. Limitation of using only the Thresholding technique is, it extracts cloud structures resulting in false large size parameters leading to the increased area during the merging of clouds [7]. Thus, the Thresholding technique may result in incorrect MCS identification and tracking while several cells are present and where the shape of the system changes rapidly. Although Source Apportionment Technique (SAT) performs better than Thresholding, it can only detect a single biggest cloud in an image if numerous cold cloud clusters are present. References [22] [23] [24], also used the KMC algorithm for MCS identification. As mentioned in [26] KMC is a widely used technique for image segmentation. Even though KMC gives good results, the value of *K* must be determined before its use, which is unknown prior to applying it for cloud segmentation. For different values of *K*, it may lead to different results [26].

To address the above-mentioned limitations of the SAT and KMC methods, their combinations with the Thresholding technique are proposed and results are analyzed against the Thresholding method. An empirical study

is done with different values of *K*, for KMC algorithm implementation by combining it with the Thresholding technique.

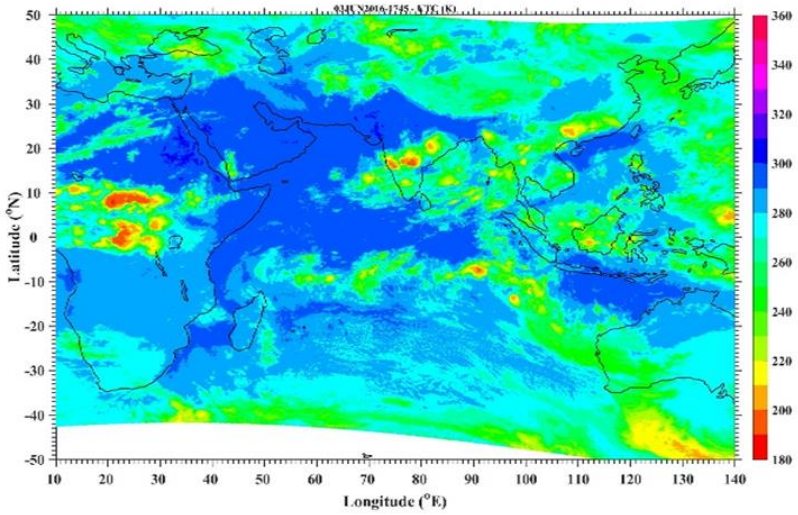

1.1. MCS identification based on Hue channel of HSV color space

The three methods, namely Thresholding, proposed method SATHT i.e. SAT combined with Thresholding, and K means clustering technique combined with Thresholding, are implemented on the Hue channel of the Hue, Saturation, and Value (HSV) color space. Color image processing makes it simple to identify the objects while extracting them from the image as it is easy to see color shades compared to grey shades [27]. In addition, color images also provide more visual information about the object [28]. Color space is mathematically modelled to represent color information as a combination of three or four color components [29]. RGB is a traditional color space with red, blue, and green components. RGB is a device-dependent color space [27], and there is a significant change in RGB components if lighting conditions change [30]. Therefore, it is unsuitable for color-based segmentation as luminance and chrominance components get mixed [31]. HSV relates closely to how humans perceive color [32]. In HSV color space, the Hue component gives the pure color value. Saturation describes the degree of white light present in the pure color and brightness of the color described by the Value component [27]. In HSV, the pixel intensity color component is easily separated and remains stable during the change in exposure or lighting conditions [31]. Hence, in this work, the Hue channel of the HSV color model is used for MCS identification instead of RGB. The advantages of the HSV color space over other color spaces are detailed in [33]. Equations (1) - (10) describe RGB to HSV conversion based on the formulas given in [32]. Here R, G, and B represent pixel-wise red, green, and blue color component values, respectively. Similarly, H, S, and V represent pixel-wise Hue, Saturation, and Value color component values, respectively.

$$P: = maximum\ of\ (R, G, B) \tag{1}$$

$$Q: = minimum\ of\ (R, G, B) \tag{2}$$

$$H = 0 \qquad if\ R = G = B \tag{3}$$

$$H = 60\ x\ \left(\frac{G-B}{P-Q}\right) \qquad if\ P = R \tag{4}$$

$$H = 120 + 60\ x\ \left(\frac{B-R}{P-Q}\right) \qquad if\ P = G \tag{5}$$

$$H = 240 + 60\ x\ \left(\frac{R-G}{P-Q}\right) \qquad if\ P = B \tag{6}$$

$$S = \frac{P-Q}{P} \qquad if\ P \neq 0 \tag{7}$$

$$S = 0 \qquad if\ P = 0 \tag{8}$$

$$V = P \tag{9}$$

S and *V* values range from 0 to 1, whereas *H* ranges from 0 to 360. Then for 8-bit values *H, S,* and *V* are mapped as

$$S = S\ x255, V = V\ x255,\ H = H/2 \quad (10)$$

After splitting the image into H, S, and V components, the Hue channel is used for further image segmentation operations to identify and extract the cold clouds. Following are the three proposed methods based on the combination of the widely used segmentation techniques of Thresholding, *K* means clustering (KMC), and Region Growing. These methods are applied to the Hue channel of HSV color space. Here, temperatures below 220K are considered since they represent deep convection.

1.2. Hue channel Segmentation based on Thresholding technique (HT)

Here Thresholding segmentation is applied to the Hue component of the HSV color model with the following steps.

Algorithm: Hue channel segmentation based on Thresholding (HT)

Input: RGB BT image $\boldsymbol{i(x,y)}$

Output: Segmented output image $\boldsymbol{o(x,y)}$

1. RGB BT image $\boldsymbol{i(x,y)}$ is converted from RGB to HSV color space. HSV image is split into hue, saturation, and value components.
2. Hue image $\boldsymbol{h(x,y)}$ is thresholded with the Hue value equivalent to the brightness temperature of 220K shown as HTH220K in (11) to generate a segmented output image $\boldsymbol{o(x,y)}$
3. For Any point $\boldsymbol{(x,y)}$ within an output image $\boldsymbol{o(x,y)}$,

   $o(\boldsymbol{x,y}) = \boldsymbol{255\ if\ h(x,y) \geq HTH22K}$

   $\boldsymbol{o(x,y) = 0\ if\ h(x,y) < HTH220K}$ (11)

All the image pixels with the Hue values above the threshold are removed, retaining only values representing the clouds with cold temperatures below 220K from the range of values from 360K to 180K.

$\boldsymbol{o(x,y)}$ represents an image consisting of foreground MCS clusters or contours representing pixels equivalent to a temperature below or equal to 220K in white color with a black background.

1.3. Hue Channel Segmentation based on SAT technique combined with Thresholding (SATHT)

This approach combines the Source Apportionment Technique (SAT) in [7] with the Thresholding technique.

Algorithm: Hue Channel Segmentation based on SAT technique combined with Thresholding (SATHT)

Input: RGB BT image $i(x,y)$

Output: Segmented output image $o(x,y)$

1. First, Hue channel Segmentation based on the Thresholding technique is performed with input RGB image $\boldsymbol{i}(\boldsymbol{x},\boldsymbol{y})$ to get thresholded image $\boldsymbol{o}(\boldsymbol{x},\boldsymbol{y})$. Here the image $\boldsymbol{o}(\boldsymbol{x},\boldsymbol{y})$ consists of MCS contours. This step is used to get the center pixels of cloud contours representing cold temperatures below 220K. These center point locations of each cloud contour act as a multiple local minimum over the entire image.
2. Center points of each cloud contour are taken as seed points, and SAT is applied on the Hue channel image $\boldsymbol{h}(\boldsymbol{x},\boldsymbol{y})$ as per the technique used in [7].
3. Pixel values representing minimum BT in a region of interest, i.e. cloud contour center points within a given image $\boldsymbol{h}(\boldsymbol{x},\boldsymbol{y})$ are selected as a seed point $\boldsymbol{P0}$.
4. Around the seed point $\boldsymbol{P0}$, each 5×5 neighboring pixel is considered pixel $\boldsymbol{P1}$.
5. Only those pixels are retained where the ratio $\boldsymbol{P1/P0} < \boldsymbol{R}$.$\boldsymbol{R}$ is chosen, so neighboring pixel values indicate temperature value below BT threshold, i.e., 220K.
6. Then $\boldsymbol{P1}$ acts as a new $\boldsymbol{P0}$. Again, step (5) is repeated until no new neighboring pixel satisfies the condition of $\boldsymbol{P1/P0} < \boldsymbol{R}$ or the new pixel value does not represent the minimum brightness temperature below the BT threshold.
7. The binary image is created with retained pixels indicating white pixels and the remaining pixels having a black background.

The SAT extracts a single MCS within an image. Multiple MCS can be found in one image, hence multiple MCS must be identified. One way of using the SAT method to extract multiple cold cloud objects is by considering every pixel as a seed point. However, it takes a very long time to execute, and it will not be efficient. To extract multiple MCS representing deep convective regions with temperatures below 220K, segmentation based on Hue channel Thresholding is applied as a first step. Then the centroids of these extracted cloud contours are passed to the SAT as a seed point beside the pixel representing minimum BT in a localized region. Here SAT is applied on the hue channel image $\boldsymbol{h}(\boldsymbol{x},\boldsymbol{y})$ with multiple seed points. As image pixels are segmented with the Thresholding Hue value representing temperature below 220K, it covers all pixels equivalent to temperatures below 220K. It avoids applying the SAT to every pixel of an image.

1.4. Hue Channel Segmentation based on *K* Means Clustering combined with Thresholding (KMCHT)

Reference [34] proposed *K* means clustering algorithm (KMC) which is widely used for image segmentation [35]. It divides data points into a fixed number of homogeneous groups called clusters. There are two steps while implementing the *K* means clustering algorithm. The first step calculates k number of cluster centers, i.e., centroids. The second step assigns each data point to the cluster with the nearest centroid. The nearest centroid is assigned based on the distance between the centroid and the respective data point. The most commonly used distance is Euclidean distance. The *K*-means method iterates until the sum of distances between each data point, and its cluster centroid is minimized. *K* means the clustering algorithm for image segmentation is explained below.

Algorithm: Hue Channel Segmentation based on K Means Clustering combined with Thresholding (KMCHT)

Input: RGB BT image $i(x,y)$

Output: Segmented output image $o(x,y)$

1. Let $\boldsymbol{i}(\boldsymbol{x},\boldsymbol{y})$ be an input image with $\boldsymbol{x} * \boldsymbol{y}$ pixels to be clustered into k clusters and $\boldsymbol{ck}$ are the cluster centers.
2. Initialize the number of clusters k as well as respective centers.
3. For every pixel of an image, calculate the Euclidean distance d as in (12), between the center points and every pixel of an image using the relation given below.

4. $\boldsymbol{d} = \|\boldsymbol{i}(\boldsymbol{x},\boldsymbol{y}) - \boldsymbol{ck}\|$ (12)
5. Assignment of all the pixels to the nearest center based on distance $\boldsymbol{d}$.
6. Once all pixels have been assigned, recalculate the new position of the cluster center with the relation given in (13) below.

   $$\boldsymbol{ck} = \boldsymbol{1/k}\sum_{y=0}^{n-1}\sum_{x=0}^{m-1}\boldsymbol{i}(\boldsymbol{x},\boldsymbol{y}) \quad (13)$$

   Where x varies from 0 to m-1, y varies from 0 to n-1
7. If no data point was reassigned, then stop, otherwise repeat steps 4 and 5.
8. Reshape the pixels of the cluster into the output image $\boldsymbol{p}(\boldsymbol{x},\boldsymbol{y})$.

On the image obtained at the output of KMC, segmentation based on Hue channel Thresholding is applied, as shown in Fig. 2.

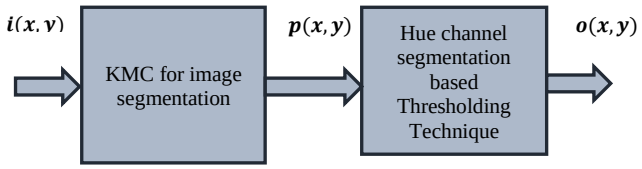

Figure 2. KMC technique combined with Hue Thresholding Technique

Here all the pixels representing the Hue value below the temperature equivalent of 220K are retained as a white foreground, and other pixels are part of the black background. The challenge with KMC is that it requires a value of K, or the number of clusters, to be determined before the clustering process can begin. Different K values are tested to address this issue. For KMC-based segmentation, the optimum value of K is chosen.

Once the segmentation is performed for all three methods, post-processing in the form of morphological operation of closing, i.e., dilation following erosion operation is performed. It is required to close the void areas generated at the output of the segmentation due to the pixels representing the map areas in the form of thin lines which didn't represent the pixel value below minimum BT criteria [36].

III. EVALUATION METHODS

The quantitative performance indicators used to compare different segmentation models are listed below [36].

1.5. Pixel Accuracy (A)

Image segmentation is considered a binary classification problem as it generates the binary mask. Here, 1 indicates the positive value i.e., a white pixel, and 0 indicates the negative value, i.e. a black pixel. Pixel accuracy is a ratio of the correctly classified or identified pixel values divided by the total number of pixels [37] as shown in (14). It ranges from 0 to 100. For MCS identification, there are two classes, white cloud clusters representing BT below 220K (True Positives) and the remaining pixels as a black background (True Negatives).

$$A = (Tp + Tn)/(Tp + Tn + Fp + Fn) \quad (14)$$

Where Tp is true positive, Tn is true negative, Fp is false positive and Fn is false negative. Computations of these values using output images representing segmented clouds and ground truth images are shown by (15) below.

$$Fp = \sum_{y=0}^{n-1}\sum_{x=0}^{m-1} if(not\ g(x,y)\ \&\ o(x,y) == 1)$$

$$Fn = \sum_{y=0}^{n-1}\sum_{x=0}^{m-1} if(g(x,y)\ \&\ not\ o(x,y) == 1)$$

$$Tp = \sum_{y=0}^{n-1}\sum_{x=0}^{m-1} if(g(x,y)\ \&\ o(x,y) == 1)$$

$$Tn = \sum_{y=0}^{n-1} \sum_{x=0}^{m-1} if(not\ g(x,y)\ \&\ not\ o(x,y) == 1) \quad (15)$$

Where x varies from 0 to m-1, y varies from 0 to n-1

$g(x,y)$ – Ground truth image pixel intensity at (x,y).

$o(x,y)$ – Output image pixel intensity at (x,y)

$(x,y) \in \{0 \le x \le m-1, 0 \le y \le n-1\}$

1.6. Mean Precision (Pr), Recall (Rc) and F1 score ($F1$)

Precision determines the percentage of the cold cloud pixels, i.e., white pixels correctly detected (True Positive) out of the total number of white pixels (total of true and false positive) within the segmented image as shown in (16). Recall determines the percentage of total correctly identified cold cloud white pixels, as shown in (17). Precision and recall are defined by referring [37] and ranges between 0 and 1.

$$\text{Pr} = Tp\ /(Tp + Fp) \quad (16)$$

$$Rc = Tp/(Tp + Fn) \quad (17)$$

F1-score is defined as the harmonic mean of precision and recall [23]. It ranges between 0 and 1.

$$F1 = 2(\text{Pr}\ x\ Rc)/(Pr + Rc) \quad (18)$$

4.1 Intersection over Union (IoU or the Jaccard Index)

IoU is defined as the area of intersection of the predicted, i.e. cold cloud white pixels within the segmented image and the ground truth image, divided by the area of the union of cold cloud white pixels within both the images [37] as in (19).

$$IoU = J(A,B) = |A \cap B|/|A \cup B| \quad (19)$$

Where A represents ground truth image, B represents predicted segmented images, and IoU ranges between 0 and 1.

IV. RESULTS AND DISCUSSION

As mentioned all three methods of MCS identification based on the Hue channel of the HSV color model are implemented on the IR BT images.

1.7. Hue channel Segmentation based on Thresholding technique (HT)

Various hue values were applied to threshold the image to select the pixel values representing the temperature below 220K, and the outcomes were compared. It was necessary to experiment with various Hue values in order to determine the ideal Hue value threshold. Several Hue threshold levels were experimented with. Ground truth images were used to evaluate the segmentation methods. Section 4 provides an explanation of the quantitative metrics used to assess segmentation performance based on HT at various Hue threshold values. Performance metric values are evaluated for each image, and the average or mean is computed for each metric over all the images.

Table 1. Evaluation metrics for Hue channel segmentation based on the Thresholding technique (HT)

Hue Value Threshold	Mean IoU	Mean Pixel_ Accuracy	Mean Precision	Mean Recall	Mean F1_ Score	Time required for execution in seconds
29	0.499	99.63	0.970	0.506	0.660	55.33
30	0.755	99.82	0.978	0.767	0.859	55.83
31	0.848	99.89	0.97	0.86	0.917	55.56
32	0.891	99.92	0.960	0.924	0.942	55.52
33	**0.893**	**99.92**	**0.930**	**0.957**	**0.943**	**55.67**
34	0.873	99.90	0.892	0.975	0.932	55.62
35	0.842	99.87	0.852	0.985	0.913	55.81
36	0.804	99.83	0.809	0.991	0.890	55.42
37	0.760	99.78	0.763	0.994	0.863	56.09
38	0.709	99.71	0.711	0.996	0.82	55.58
39	0.631	99.59	0.632	0.997	0.771	60.26
40	0.52	99.36	0.527	0.998	0.686	55.72

Table 1 shows the mean values of IoU and all other metrics such as Pixel accuracy, Precision, Recall, and F1-Score are good at the Hue threshold of 33. IoU measures the similarity between the ground truth and the output images. IoU is considered a more reliable metric for image segmentation and object detection [38]. Mean IoU is good (0. 893) with a Hue threshold of 33. With further increase in Hue threshold value IoU and other metrics values decrease. Thus, Hue threshold value 33 is used further to compare the results with SATHT and KMCHT.

1.8. Selection of *k* value for Hue Channel Segmentation based on *K* Means Clustering combined with Thresholding (KMCHT)

The value of k, i.e. number of clusters, is an important parameter for K means clustering implementation as its value significantly impacts the results obtained. At different k values, the segmentation performance of KMCHT is evaluated using quantitative metrics. Each image's performance metric values were analyzed, and an average or mean was computed for each metric over all images. These metric values are shown in Table 2. It is seen that Mean values of IoU and all other metrics such as Pixel accuracy, Precision, Recall, and F1-Score are good at k equal to 47. Though the *k* value is increased further, IoU oscillates around 0.83. It is seen that optimum results are at K = 47 with respect to execution time. As the *k* value increases further, there is no significant performance gain. However, execution time increases. Therefore, the value of *k* is chosen as 47 for the segmentation based on KMCHT.

Table 2. Evaluation metrics for *K*-means cluster with different values of *k*

k	Mean IoU	Mean Pixel_ Accuracy	Mean Precision	Mean Recall	Mean F1_Score	Time required for execution in seconds
21	0.666	99.74	0.851	0.786	0.773	6594.69
25	0.755	99.80	0.837	0.897	0.850	7743.72
30	0.786	99.83	0.847	0.926	0.872	8934.56
35	0.808	99.84	0.842	0.955	0.891	10347.67
40	0.816	99.84	0.851	0.955	0.896	12876.97
41	0.816	99.84	0.851	0.955	0.896	11960.48
42	0.822	99.85	0.848	0.964	0.901	12226.44
43	0.826	99.85	0.853	0.964	0.904	12573.16
44	0.823	99.85	0.858	0.955	0.901	12841.94
45	0.821	99.85	0.852	0.959	0.899	13407.13
46	0.83	99.86	0.86	0.961	0.906	13509.61
47	**0.831**	**99.86**	**0.862**	**0.96**	**0.906**	**13673.36**
48	0.828	99.86	0.855	0.964	0.905	13998.92
49	0.831	99.86	0.858	0.964	0.907	14258.06
50	0.83	99.86	0.86	0.962	0.906	14595.54

1.9. Hue Channel Segmentation based on SAT technique combined with Thresholding (SATHT)

As seen in the method SATHT, P0 is taken as a seed pixel. The ratio of $P1/P0$ is calculated where P1 is a neighboring pixel within 5x5 pixels around P0. For retention of the pixels representing temperature below 220K, parameter R is taken such that $P1/P0 < R$. The value of R is selected empirically by testing different R values and observing the performance of each R as shown in Table 3. After R = 4, there is a minimal variation in the values of the performance metrics. Therefore, R values are taken in the multiples of 5. It has been observed from R = 35 that there is no increase in the values of the performance metrics. Therefore, R is selected as 35.

1.10. Evaluation of different techniques

The performance of all three methods is evaluated for each of the calculated metric values. Fp, Fn, Tp and Tn values are computed using (15) and are used to calculate the performance metrics. As given in Tables 1, 2, and 3 mean performance metrics values calculated over all images are shown as Mean IoU, Mean Pixel Accuracy, Mean

Precision, Mean Recall, and Mean F1 score along with execution time.

Table 3. Evaluation metrics for SATHT with different values of *R*

Value of *R*	Mean IoU	Mean Pixel_ Accuracy	Mean Precision	Mean Recall	Mean F1_ Score	Time required for execution in seconds
1	0.114	99.32	0.974	0.114	0.199	253.22
2	0.842	99.87	0.922	0.907	0.913	260.11
3	0.865	99.89	0.922	0.934	0.927	284.91
4	0.882	99.90	0.922	0.953	0.936	301.89
5	0.884	99.91	0.922	0.954	0.937	322.43
10	0.888	99.91	0.922	0.959	0.940	488.04
15	0.888	99.91	0.922	0.960	0.940	512.60
20	0.891	99.91	0.922	0.96	0.942	548.92
25	0.891	99.91	0.922	0.964	0.942	586.11
30	0.892	99.91	0.922	0.964	0.942	603.52
35	**0.893**	**99.91**	**0.922**	**0.966**	**0.943**	**639.04**
40	0.893	99.91	0.922	0.966	0.943	682.02
45	0.893	99.91	0.922	0.966	0.943	660.11
50	0.893	99.91	0.922	0.966	0.943	687.94
55	0.893	99.91	0.922	0.966	0.943	668.85
60	0.893	99.91	0.922	0.966	0.943	677.76
65	0.893	99.91	0.922	0.966	0.943	646.51
70	0.893	99.91	0.922	0.966	0.943	638.92

The best results for these performance metrics are obtained for the Thresholding method with a Hue value threshold of 33, for the K-means cluster with a value K of 47, and metrics for SATHT values R of 35. These results are shown in Fig. 3 to 4.

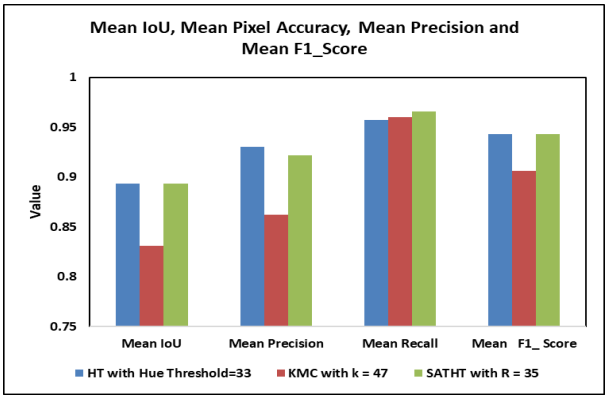

Figure. 3. Mean IoU, Mean Precision, Mean Recall and Mean F1 Score for cold cloud segmentation applied in Fig. 1 using HT, KMCHT, and SATHT

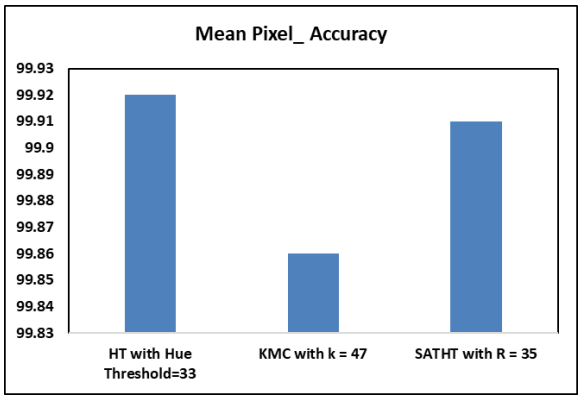

Figure 4. Mean Pixel Accuracy cold cloud semantic segmentation applied in Fig. 1 using HT, KMCHT, and SATHT

From these charts, both HT and SATHT give better results than the MCHT method. Both these techniques produce similar results in terms of the mean values of performance metrics over all images. The execution time required for the HT, SATHT, and KMCHT is 55.67 seconds, 548.92 seconds, and 13,673.36 seconds respectively. As SATHT and KMCHT are iterative, execution time is high. For SATHT as only contour centers are taken as seed points, relative execution time is less as compared to KMCHT. As the nature of cloud cluster formation is non-deterministic with many smaller MCSs during initiation and dissipation stages for MCS life cycle study, where the number of clusters varies rapidly, KMCHT is not useful. As compared to SATHT, the HT method is more sensitive to the pixel intensities making it susceptible to noise. Small variations in the intensity values may affect the segmentation output. If the temperature gets changed from 220K to 200K to consider more deep convection it needs more manual efforts and becomes tedious to find the optimum value of the threshold for HT. Here only advantage of using HT is faster execution. If images are generated with a duration of 30 minutes it becomes beneficial to use the proposed SATHT method for the cold cloud segmentation as it gives more stable output.

1.11. Qualitative Analysis

As clouds get formed with indefinite shapes and sizes, it becomes tedious as well as a time-consuming job to create its ground truth manually, therefore for the analysis, 15-20 images from each month of 2016 were chosen based on varying shapes and cloud counts per image. As an example, Fig. 1 shows the typical BT measurements from Kalpana-1 on June 3, 2016, at 1745 UTC. Fig. 5 to 8 show the ground truth image, as well as outputs of the methods KMCHT, SATHT, and HT, respectively, for the RGB image shown in Fig. 1 From Fig. 5 and 7, KMCHT showed a few extra contours unrelated to pixels representing below 220K. The Mean Intersection of Union (MIoU) performance parameter for KMCHT is around 0.83, whereas for SATHT and HT it is above 0.89. Ideally, it should be 1. Therefore, it can be concluded that SATHT and HT methods give better output than KMCHT.

It is crucial to detect the MCS accurately as significant features such as cloud area, location, and direction of movement can further be extracted while processing MCS tracking. The true detection of MCS leads to correct lifetime estimation and investigation of their characteristics. Therefore, a better characterization of MCS would help to improve the numerical weather forecasting capabilities.

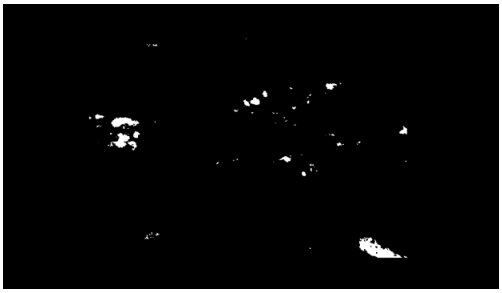

Figure 5. Ground Truth Image of the segmentation of clouds below 220K for Fig. 1

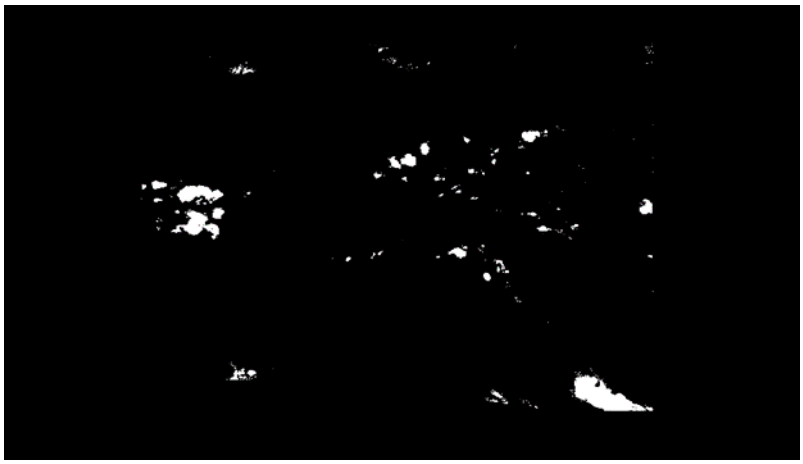

Figure 6. Segmentation of clouds below 220K using HT of Fig. 1

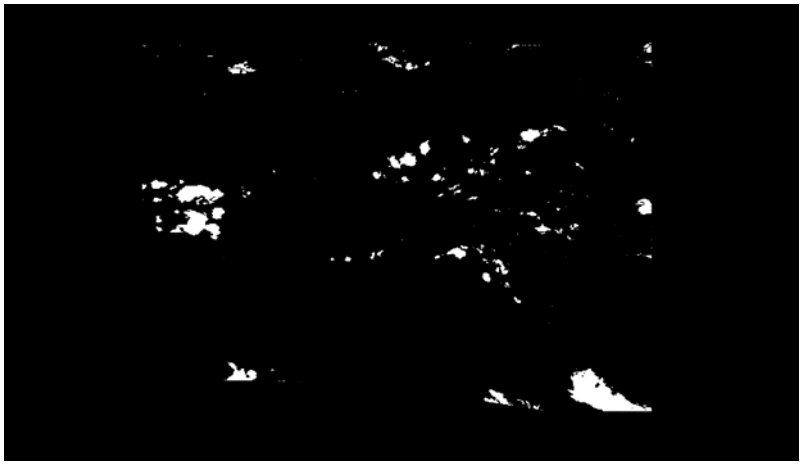

Figure 7. Segmentation of clouds below 220K using KMCHT of Fig. 1

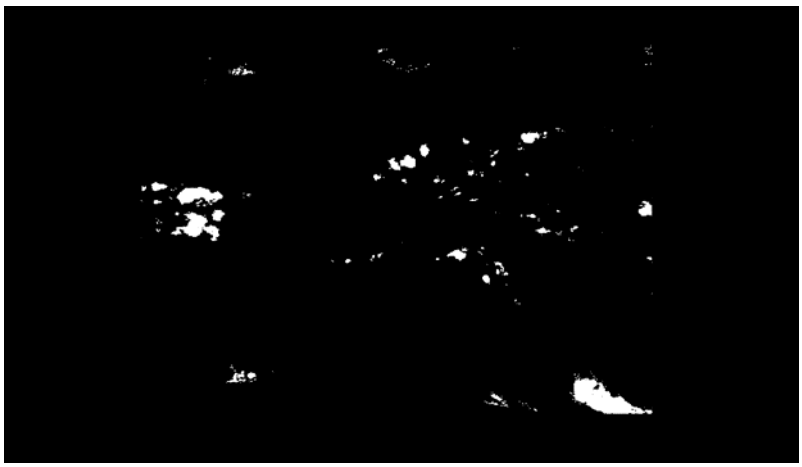

Figure 8. Segmentation of clouds below 220K SATHT of Fig. 1

V. CONCLUSION

This research presents three Hue channel-based algorithms for MCS identification utilizing RGB images based on IR brightness temperature. The techniques employed include the Hue channel segmentation based on the Thresholding technique (HT), the proposed Hue channel segmentation based on the SAT technique combined with Thresholding (SATHT), and the Hue channel segmentation based on K Means Clustering coupled with Thresholding (KMCHT). The goal of this work is to assess the effectiveness of MCS identification strategies so that the optimal method may be used.

These approaches' effectiveness is assessed using performance metrics like Mean IoU, Mean Pixel Accuracy, Mean Precision, Mean Recall, and Mean F1 Score. The Hue value threshold of 33 produces the best results for the HT technique. With a quick execution time of about 56 seconds, it is more sensitive as well as tedious to get the optimum threshold value. It has been noted that SATHT produces superior MCS cloud detection outcomes compared to HT and KMCHT approaches considering more robust and stable output. With a dataset of 200 images, using SATHT the performance metrics Mean IoU, Mean Pixel Accuracy, Mean Precision, Mean Recall, and Mean F1 Score, are 0.893, 99.91, 0.922, 0.966, and 0.943, respectively.

The accurate cloud identification step is an important factor for accurate MCS tracking. The SATHT approach provides the best results for accurate MCS cloud identification over other techniques. The results of traditional segmentation algorithms provide an edge over the advanced techniques of Deep Learning techniques against the cost of the requirement of huge labeled satellite image data and computational power. This justifies the usage of traditional techniques for MCS detection using segmentation. This work will be expanded further to track MCS for better forecasting and nowcasting.

Acknowledgment

The Kalpana-1 data obtained from the Meteorological and Oceanographic Satellite Data Archival Centre (MOSDAC) website (http://www.mosdac.gov.in) is gratefully acknowledged.

Author contributions

Vidya Patil: Conceptualization, Methodology, Software, Experimentation, Resources, Validation, Writing – original draft, **Anuradha Phadke:** Formal analysis, Investigation, Writing – review and Editing,

Subrata Kumar Das: Data curation, Formal analysis, Investigation, Writing – review and Editing.

Conflicts of interest

The authors declare no conflicts of interest.

REFERENCES

[1] R. A. Houze Jr., "Mesoscale convective systems," Reviews of Geophysics, Vol. 42, No. 4, pp. RG4003-1–RG4003-43, Dec. 2004.

[2] Z. Feng, L. R. Leung, R. A. Houze, S. Hagos, J. Hardin, Q. Yang, B. Han, and J. Fan, "Structure and evolution of mesoscale convective systems: Sensitivity to cloud microphysics in convection-permitting simulations over the United States," Journal of Advances in Modeling Earth Systems, Vol. 10, No. 7, pp. 1470–1494, Jul. 2018.

[3] R.S. Schumacher, and K.L. Rasmussen, "The formation, character and changing nature of mesoscale convective systems", Nature Reviews Earth & Environment, Vol. 1, pp. 300–314, Jun. 2020.

[4] X. Huang, C. Hu, Xing Huang, Y. Chu, Y. Tseng, G. J. Zhang, and Y. Lin, "A long-term tropical mesoscale convective systems dataset based on a novel objective automatic tracking algorithm," Climate Dynamics, Vol. 51, pp. 3145–3159, Jan. 2018.

[5] R A. Maddox, "Mesoscale convective complexes." Bulletin of the American Meteorological Society, Vol. 61, No. 11, pp. 1374–1387, Nov. 1980.

[6] R. A. Houze Jr.uf , "100 years of research on mesoscale convective systems," Meteorological Monographs, Vol. 59. No. 1, pp. 17.1–17.54, Jan. 2018.

[7] B. P. Shukla and P. K. Pal, "A Source Apportionment Approach to Study the Evolution of Convective Cells: An Application to the Nowcasting of Convective Weather Systems", IEEE Journal of Selected Topics in Applied Earth Observations and Remote Sensing, Vol. 5, No. 1, pp. 242–247, Feb. 2012.

[8] T. Fiolleau and R. Roca, "An Algorithm for the Detection and Tracking of Tropical Mesoscale Convective Systems Using Infrared Images From Geostationary Satellite", IEEE Transactions on Geoscience and Remote Sensing, Vol. 51, No. 7, pp. 4302–4315, Jul. 2013.

[9] A. G. Laing and J. M. Fritsch, "The global population of mesoscale convective complexes," Quarterly Journal of the Royal Meteorological Society, Vol. 123, No. 538, pp. 389– 405, Jan. 1997.

[10] S. Rafati and M. Karimi, “Assessment of mesoscale convective systems using IR brightness temperature in the southwest of Iran”, Theoretical and Applied Climatology, Vol. 129, pp. 539–549, Jul. 2017.

[11] D.A. Vila, L.A.T. Machado, H. Laurent, and I. Velasco, “Forecast and Tracking the Evolution of Cloud Clusters (ForTraCC) Using Satellite Infrared Imagery: Methodology and Validation”, Weather and Forecasting, Vol. 23, No. 2, pp. 233–245, Apr. 2008.

[12] K. Whitehall, C.A. Mattmann, G.Jenkins, M. Rwebangira, B. Demoz, D. Waliser, J. Kim, C. Goodale, A. Hart, P. Ramirez, M.J. Joyce, M. Boustani, P. Zimdars, P. Loikith, and H. Lee, “Exploring a graph theory based algorithm for automated identification and characterization of large mesoscale convective systems in satellite datasets”, Earth Science Informatics, No. 8, pp. 663–675, Sep. 2015.

[13] V. Patil, S. K. Das, and A. Phadke, “Methods for Mesoscale Convective Systems Detection and Tracking: A Survey”, presented at the *10th International Conf. On Computing, Communication and Networking Technologies (ICCCNT)*, Kanpur, India, Jul. 06-08, 2019.

[14] C. Morel and S. Senesi, “A climatology of mesoscale convective systems over Europe using satellite infrared imagery. I: Methodology”, Quarterly Journal of the Royal Meteorological Society, Vol. 128, No. 584, pp. 1953–1971, Jul. 2002.

[15] C. Klein, D. Belušić, and C.M. Taylor, “Wavelet Scale Analysis of Mesoscale Convective Systems for Detecting Deep Convection from Infrared Imagery”, Journal of Geophysical Research Atmospheres, Vol. 123, No. 6, pp. 3035–3050, Mar. 2018.

[16] A. Makris and C. Prieur, “Bayesian Multiple-Hypothesis Tracking of Merging and Splitting Targets”, IEEE Transactions on Geoscience and Remote Sensing., Vol. 52, No. 12, pp. 7684–7694, Dec. 2014.

[17] A. Rehbein, T. Ambrizzi, and C.R. Mechoso, “Mesoscale convective systems over the Amazon basin. Part I: climatological aspects”, International Journal of Climatology, Vol. 38, No.1, pp. 215–229, Jan. 2018.

[18] B. Goswami, G. Bhandari, and S. Goswami, “Mesoscale convective system tracking in satellite thermal infrared images”, presented at the *Annual IEEE India Conference (INDICON)*, Pune, India, Dec. 11-13, 2014.

[19] A. T. Hartman, “Tracking mesoscale convective systems in central equatorial Africa,” International Journal of Climatology, Vol. 41, No. 1, pp. 469–482, Jan. 2021.

[20] C.M. Taylor, A.H. Fink, C. Klein, D.J. Parker, F. Guichard, P.P. Harris, and K. R. Knapp, “Earlier Seasonal Onset of Intense Mesoscale Convective Systems in the Congo Basin Since 1999”, Geophysical Research Letters., Vol. 45, No. 24, pp. 13,458-13,467, Dec. 2018.

[21] R. Roca and T. Fiolleau, “Extreme precipitation in the tropics is closely associated with long-lived convective systems”, Communications Earth & Environment, Vol. 1, No. 18, Sep. 2020.

[22] A.K. Mandal, S. Pal, A.K. De and S. Mitra, “Novel approach to identify good tracer clouds from a sequence of satellite images”, IEEE Transactions on Geoscience and Remote Sensing, Vol. 43, No. 4, pp. 813–818, Apr. 2005.

[23] B. Goswami and G. Bhandari, “Automatically adjusting cloud movement prediction model from satellite infrared images” presented at the *Annual IEEE India Conference*, Hyderabad, India, Dec. 16-18, 2011.

[24] B. Goswami and G. Bhandari, “Convective Cloud Detection and Tracking from Series of Infrared Images”, Journal of the Indian Society of Remote Sensing, Vol. 41, pp. 291–299, Jun. 2013.

[25] J.-B. Courbot, V. Duval, and B. Legras,"Sparse analysis for mesoscale convective systems tracking", Signal Processing: Image Communication, Vol. 85, 115854, Jul. 2020

[26] M. Ahmed, R. Seraj, and S.M.S. Islam,” The k-means Algorithm: A Comprehensive Survey and Performance Evaluation”, Electronics, Vol. 9, No. 8, 1295, Aug. 2020.

[27] 4th ed., Gonzalez, Woods, Digital Image Processing: Colour Image Processing, New York, NY, USA: Pearson, 2018, pp. 400-420.

[28] A. Jain, Fundamentals of Digital image processing, Englewood Cliffs, NJ 07632, USA: Prentice Hall, 1989, pp. 60-71.

[29] K.B. Shaik, P. Ganesan, V. Kalist, B.S. Sathish, and J.M.M. Jenitha, “Comparative Study of Skin Color Detection and Segmentation in HSV and YCbCr Color Space”, Procedia Computer Science, Vol. 57, pp. 41–48, Aug. 2015.

[30] C. Lv, J. Li, Q. Kou, H. Zhuang, and S. Tang, “Stereo Matching Algorithm Based on HSV Color Space and Improved Census Transform”, Mathematical Problems in Engineering, Vol. 2021, Jul. 2021.

[31] Ganesan P and V. Rajini, "Assessment of satellite image segmentation in RGB and HSV color space using image quality measures,” presented at the *International Conference on Advances in Electrical Engineering (ICAEE),* Vellore, India, Jan. 09-11, 2014.

[32] N.A. Ibraheem, M.M. Hasan, R.Z. Khan, and P.K Mishra, “Understanding color models: a review”, ARPN Journal of Science and Technology, Vol. 2, No. 3, pp.265-275, Apr. 2012.

[33] K. Plataniotis, and A.N. Venetsanopoulos, Color image processing and applications, Springer-Verlag, 2000, pp. 25-32.

[34] J. A. Hartigan, and M. A. Wong, “A K-means clustering algorithm,” Journal of the Royal Statistical Society, vol. 28, no. 1, pp. 100–108, 1979.

[35] N. Dhanachandra, K. Manglem, and Y.J. Chanu, “Image Segmentation Using K -means Clustering Algorithm and Subtractive Clustering Algorithm”, Procedia Comput. Sci., Vol. 54, pp. 764–771, Aug. 2015

[36] M. Gao, X. Wang, S. Zhu, and P. Guan, “Detection and segmentation of cement concrete pavement potholes based on image processing technology,” Mathematical Problems in Engineering, Vol. 2020, pp.1-13, Jan. 2020.

[37] S. Minaee, Y. Boykov, F. Porikli, A. Plaza, N. Kehtarnavaz, and D. Terzopoulos, “Image Segmentation Using Deep Learning: A Survey”, IEEE Transactions on Pattern Analysis and Machine Intelligence, Vol. 44, No. 7, pp. 3523–3542, Jul. 2022.

[38] L. Li, X. Li, L. Jiang, X. Su, and F. Chen, “A review on deep learning techniques for cloud detection methodologies and challenges”, Signal, Image and Video Processing, 15, pages1527–1535, Apr. 2021.

[39] https://www.mosdac.gov.in/ kalpana-1-data-products